# Electronic structure and properties of Li-insertion materials: $Li_2RuO_3$ and $RuO_2$

M. D. Johannes, A. M. Stux, and K. E. Swider-Lyons
*Naval Research Laboratory, Washington, D.C. 20375, USA*

(Received 27 September 2007; revised manuscript received 3 January 2008; published 25 February 2008)

We synthesize, measure, and use first principles density functional theory calculations to study two Ru-based metal oxides, layered $Li_2RuO_3$ and rutile $RuO_2$, in terms of their electrochemical performance as potential battery cathode materials. Despite being composed of identical constituent elements, and having the same local structure ($RuO_6$ octahedra), the two compounds have very different voltage profiles and conductivities that can be traced back to differences in their long range structures. We find that three basic factors contribute to the superior cathode properties of $Li_2RuO_3$ in comparison to $RuO_2$: a lower Ru/O ratio that raises the oxidation state of Ru, more localized electron states and longer Li-Li distances due to quasi-two-dimensionality, and strong Ru-Ru bonding in the metal-oxide plane that shifts the electronic energy levels. The principles extracted from the comparison of these two materials are generalizable and can be used to help guide the search for superior cathode compounds.

DOI: 10.1103/PhysRevB.77.075124 PACS number(s): 71.20.Tx, 71.20.Be

## INTRODUCTION

Rechargeable Li-ion batteries are a staple of consumer electronics, such as cell phones, laptops, and music players. The high energy density and low mass/energy ratio exhibited by this class of batteries are essential for small, portable devices, but these qualities are also desirable for larger-scale applications such as power tools or car batteries. To satisfy the continuing demand for smaller and lighter electronics or for longer lasting vehicles and tools, there has been a wide scale effort to develop better Li-ion batteries by increasing both the operating voltage and capacity. In large part, these properties are controlled by the choice of the cathode. An ideal cathode will be able to accomodate a large amount of Li ions per unit weight, will operate at a high and consistent voltage, and will maintain its structural integrity throughout the charge and discharge cycles. The standard of Li-ion battery cathodes is currently $LiCoO_2$, which can reversibly intercalate approximately 0.5 Li ions per Co ion at ~3.7 V with a reasonably flat voltage profile. $LiCoO_2$, however, is expensive and environmentally unfriendly. The search for new cathode materials with superior electrochemical properties has proceeded not only experimentally, but also theoretically through the use of density functional theory to predict cathode properties prior to synthesis. Quantities such as intercalation potential, Li-ion diffusion rates, and capacity can be accurately modeled using first principles methodologies. This saves time and money by eliminating inferior cathode materials from consideration before the expensive process of synthesis, and also allows insight into the microscopic structural, chemical, and electronic factors that contribute to good cathode performance.

Two of the most important characteristics of a cathode are its intercalation potential (voltage) vs the anode, and its capacity (amount of Li it can exchange). The intercalation potential depends on the chemical potential of a Li ion in the anode compared to the chemical potential of an intercalated Li ion in the cathode. Once enough Li has entered the host lattice of the cathode to make the intercalation potential zero, the full capacity of the cathode has been reached. Given a standard anode such as Li metal, the potential and capacity will be determined by the chemical composition and structure of the cathode material. Previous work on cathode materials containing $3d$ transition-metal elements has shown that, holding the structure constant, the intercalation potential essentially tracks with the atomic number of the electrochemically active metal ion.[1,2] Here, we investigate the conjugate problem of how structure affects the intercalation potential when the constituent elements are identical. We use layered $Li_2RuO_3$ and rutile $RuO_2$ because the two compounds share nearly identical local structures, $RuO_6$ and $LiO_6$ octahedra, in addition to having the same chemical elements. We find that the layered structure of $Li_2RuO_3$ gives rise to a higher average intercalation potential, a significantly flatter discharge slope, and can accomodate slightly more Li than rutile $Li_xRuO_2$. $RuO_2$, however, has a much higher electronic conductivity. We show that three factors are important to explain the superior voltage profile and decreased conductivity of layered $Li_xRuO_3$ vs rutile $Li_xRuO_2$: (i) its lower Ru/O ratio that leads to a higher oxidation state, (ii) its lower dimensionality (quasi-two-dimensional vs fully three-dimensional), and (iii) significant metal-metal bonding between Ru atoms. Although Ru is a precious metal and, therefore, expensive, the general lessons acquired from this study are transferrable to the wider search for new cathode materials.

## I. STRUCTURE

$Li_2RuO_3$ has a layered structure much like other common layered cathode materials such as $LiCoO_2$ or $LiNiO_2$ where the transition-metal ions form a planar triangular arrangement and sit in an octahedral cage of O atoms. Li ions are intercalated between the transition-metal-oxide planes. However, in $Li_2RuO_3$, one out of every three planar Ru atoms is replaced by Li, resulting in a planar honeycomb arrangement of Ru atoms with Li atoms in the center. The overall symmetry is monoclinic ($C2/c$) and remains so as Li is deintercalated until a phase transition to rhombohedral symmetry ($R3$) occurs[3] for the compound $Li_{0.9}RuO_3$. Because phase

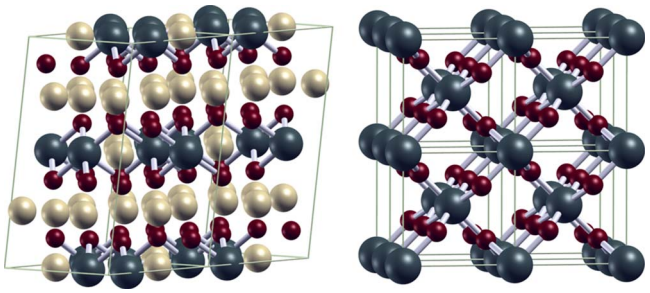

FIG. 1. (Color online) The structures of layered $Li_2RuO_3$ (left) and rutile $RuO_2$ (right). Large dark (blue) spheres are Ru ions, smaller dark (red) spheres are oxygen, and small light (yellow) spheres are Li.

transitions can be very detrimental to cathode performance, it is encouraging that a full 1.1 electrons can be withdrawn from the structure while the host remains in the $C2/c$ space group. The rutile ($C4$) structure of $RuO_2$, like layered $Li_2RuO_3$, has basic building blocks of $RuO_6$ octahedra, but takes a very different, three-dimensional structure as shown in Fig. 1. Li can be intercalated into the octahedral sites between adjacent $RuO_6$ octahedra.[4,5] However, there is an alternative, nontopotactic reaction, $4Li+RuO_2 \rightarrow 2Li_2O+Ru$ (metal), that is energetically favorable. Experimentally, both processes occur and are reversible.[5]

## II. COMPUTATIONAL DETAILS

All of our first principles calculations were done using the projector augmented plane-wave formulation[6,7] of the Vienna *ab initio* simulation program (VASP).[8] Exchange and correlation effects were accounted for using the GGA-PW91 functional[9] and all calculations were carried out in the spin-polarized framework. For the three-dimensional rutile structure, a $k$-point mesh of $16\times16\times16$ was used, whereas for the layered structure, a mesh of $16\times8\times16$ was used. The energy cutoff was set at 875 eV to allow for a high precision relaxation. Convergence with respect to both $k$-point mesh and energy cutoff was verified. To calculate the intercalation potential at various Li concentrations, we used the prescription of Ceder *et al.*[10] Although for many battery materials it is necessary to apply the LDA+$U$ (where LDA is local density approximation) (or GGA+$U$, where GGA is generalized gradient approximation) extension to the standard density functional methodology in order to obtain accurate potentials, the results presented here did not use this procedure. The cations of traditional battery materials are usually 3$d$ elements that can have strong correlation effects requiring a correction to GGA,[11] but the electrochemically active states of Ru are from the 4$d$ row, which has significantly less correlation.

We use a full structural relaxation for each separate Li concentration of each studied compound. Our calculations accurately reproduce the experimental structures reported for $Li_2RuO_3$ (Refs. 3, 12, and 13) and $RuO_2$ (Refs. 4 and 14) with good accuracy (approximately 3% error by volume). The theoretical (experimental) lattice parameters for $Li_2RuO_3$ are (in Å) $a=4.94$ (4.92), $b=8.86$ (8.77), and $c=9.88$ (10.01). For $RuO_2$ the theoretical (experimental) lattice parameters are (in Å) $a=4.56$ (4.49), and $c=3.11$ (3.12). We find that the layered compound shrinks with increasing $x$, as the negatively charged oxide planes pull in toward the positive Li plane. In contrast, the rutile structure expands as Li is added. Structural information for the specific Li concentrations we studied has not been reported, but both these facts are in agreement with observed trends.[3,4,13] We calculate the difference in the total energies of the monoclinic and rhombohedral structures of $Li_xRuO_3$ [using the lower symmetry cell ($C2/c$) for both calculations] at $x=1.0$ and $x=0.5$. The monoclinic structure is favored at $x=1.0$ by 91 meV and the rhombohedral structure is favored at $x=0.5$ by 145 meV. This indicates that the phase transition occurs for $x$ in the range $1<x>0.5$, and likely toward the high end, which agrees with the measured transition at $x=0.9$.

## III. EXPERIMENTAL DETAILS

$Li_2RuO_3$ was synthesized by mixing commercially available powders of $RuO_2$ and $Li_2CO_3$ following previously described procedures.[3,15] Briefly, hydrous $RuO_2$ (Alfa Aesar) was dried at 400 °C for 18 h to remove structural water. Afterwards, the $RuO_2$ (Alfa Aesar) was ground together with an equimolar amount of $Li_2CO_3$ (Alfa Aesar), pelletized, and sintered in air at 950 °C for 24 h. The pellets were then pulverized using an agate mortar and pestle and sieved to approximately 30 $\mu$m. Cathodes were prepared using $RuO_2$ (Alfa Aesar) and $Li_2RuO_3$, respectively, as the active $Li^+$ insertion constituent for the two types of slurries.

The active materials were formulated into slurries close to previously developed recipes.[16] The $RuO_2$ cathode slurry was a mixture of approximately 85 wt % $RuO_2$ with 3% polyvinylidene fluoride (PVDF, Atofina), 4% Super P carbon (Ensaco), and 8% KS6 carbon (Timcal). The $Li_2RuO_3$ slurry was a mixture of approximately 91 wt % $Li_2RuO_3$, 2% Super P, 4% KS6, and 3% PVDF. For both electrode slurries, the PVDF was dissolved separately in 1-methyl-2-pyrrolidone (NMP, Aldrich) and then combined with the active material/carbon powders to make a viscous ink for efficient deposition. A coating comprised of 10% fine carbon black particles (Super P) and 90% PVDF in NMP was deposited on foil current collectors to serve as a conductive coating and adhesion layer.

The slurries were deposited on current collectors of aluminum foils (All-Foils, Inc.) approximately $4\times4$ mm$^2$ in area. First, the Al and Cu foils were pretreated by etching with 1$M$ potassium hydroxide and 1$M$ nitric acid solutions, respectively, followed by rinsing with water and then acetone. Then, a layer of the conductive carbon was then added to their surfaces. The conductive coating/adhesion layer was dried on a hot plate at the lowest heat setting for approximately 1 min in order to obtain a homogeneous film. The cathode slurries were then deposited on the Al foils, respectively. The electrodes were subsequently dried again on the hot plate, and then vacuum-dried overnight at 90–95 °C before transferring to an argon-filled glovebox. The weight of

the active materials in the coatings was approximately 1 mg for the cathodes. For these Li test cells, the metallic Li foil was fixed to the Cu foil to form the anode, whereby the Li could be used as both a counter and a reference electrode.

The cathodes were evaluated in packaged Li cells at room temperature both using metallic Li. The electrolyte was $1M$ $LiPF_6$ in a mixture of carbonates containing ethylene carbonate, propylene carbonate, ethyl methyl carbonate, and diethyl carbonate. The small, packaged Li cells were assembled in the following manner: a microporous polymer film (Celgard 2730) was used as a separator and sandwiched between the active cathode material/carbon/aluminum and Li/copper electrodes. The cathode/separator/anode sandwiches were first held together by impulse sealing them in a transparent polymer bag (Saranex SX 23-P), followed by sealing in another pouch of a trilayer polyethylene-aluminum-polyester. During the sealing process, small holes were left in the polymer seals to allow electrolyte injection. After the battery was filled with the electrolyte, the pouch was fully sealed. With this packaging process, the Li cells were gently held together with no additional pressure on the electrodes. The electrochemical testing of Li-ion cells was conducted using a battery tester (Maccor 2300) set to cutoff voltages. For cells with the Li anodes, the cutoff voltages were 2.0 and 4.2 V. Cells were discharged at a $C/5$ rate (about 25–35 $\mu$A) corresponding to constant currents of 0.15–0.22 mA/cm$^2$.

## IV. INTERCALATION POTENTIAL (VOLTAGE)

We follow the formulation of Ref. 10 and calculate an average intercalation potential as

$$\bar{V}(\bar{x}) = -\frac{E_{\mathrm{Li}_{x_2}\mathrm{RuO_3}} - E_{\mathrm{Li}_{x_1}\mathrm{RuO_3}} - (x_2 - x_1)E_{\mathrm{Li}}}{x_2 - x_1}, \qquad (1)$$

where $x_2$ is assumed to be greater than $x_1$, and $\bar{x}=\frac{x_1+x_2}{2}$ is the Li concentration to which we assign the average calculated potential. The numerator contains the total energies of the indicated compounds and of metallic bcc Li (for the rutile compound, $Li_xRuO_2$ is substituted for $Li_xRuO_3$ in the total energy subscripts). We have calculated total energies for rutile $Li_xRuO_2$ and layered $Li_xRuO_3$ at $x=2.0$, 1.0, 0.5, and 0.0. The results are plotted in Fig. 2. For both compounds, the potential decreases nonmonotonically as a function of Li concentration, $x$. This nonintuitive (and unphysical) result can be explained as an artifact of our calculational technique. The ordering of the Li ions within the lattice can be quantitatively evaluated only for compounds with integer values of $x$. For the layered compound at $x=2$, the Li atoms sit at the $4d$ and $4e$ Wyckoff positions in the $C2/c$ unit cell; for $x=1$, the lowest energy state occurs when they sit at only $4e$ positions. For the rutile compound at $x=1$, the Li atoms sit at the $4c$ Wyckoff positions. For all other $x$ values in either compound, there is no good way of theoretically determining where the Li ions sit. To avoid creating large unit cells, we used the same unit cells as for the fully lithiated compounds, removed the appropriate number of Li ions (this lowered the symmetry in all cases), and then re-relaxed the cell. Intercalation potentials that are calculated using differences taken between points $x_2$ and $x_1$, where the Li positions within the respective lattices are integers for both $x$ values, give reliable and consistent results; these points are marked by filled square symbols in Fig. 2. For $x$ values corresponding to compounds with unknown Li positions, a best guess configuration was used and then relaxed computationally. It is always possible (and usually likely) that a lower energy configuation than the chosen one exists, although a larger unit cell might be required to model it. If the intercalation potential is calculated using the $x_2$ value from a compound with an unknown Li configuration and $x_1$ from a compound with a known configuration, the energy difference will be too large, resulting in an artificially high voltage. If, on the other hand, the $x_2$ value is an integer and $x_1$ is noninteger, the voltage will be shifted artificially low. In Fig. 2, the former situation occurs for the voltages shown at $\bar{x}=0.75$ and $\bar{x}=1.25$, while the latter situation occurs for the voltages shown at $\bar{x}=0.25$. The discrepancy between the voltages calculated from integer $x$ values and those calculated from noninteger $x$ values provides some idea of how much effect the Li ordering has on the total energy. In $Li_xRuO_3$, the energy of different configurations is apparently rather small. This is consistent with the relatively unconstrained two-dimensional space into which the Li ions are intercalated. Unsurprisingly, in rutile $Li_xRuO_2$, where the space for Li ions is far more constrained, the energetics has a stronger dependence on the specific Li configuration as can be seen by the larger deviation between the two kinds of points. In reality, the Li ions may be partially or fully disordered. A cluster expansion could be used to model the Li plane where such disorder occurs, and could also be useful where the Li ions are fully ordered,[17,18] but we do not use this technique here.

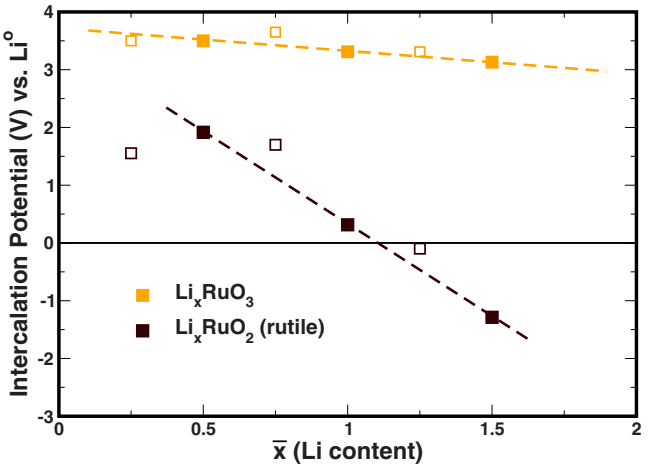


FIG. 2. (Color online) Calculated intercalation potentials $\bar{V}$ for $Li_xRuO_3$ and rutile $Li_xRuO_2$. The data points marked with filled squares correspond to calculations with no ambiguity in Li positions, while points marked with empty squares are calculations involving one lattice with unknown Li positions. The dashed lines are a guide for the eye to follow the trend of the potential along only the points with Li orderings that are certain (see text). Potentials are calculated according to Eq. (1) with the anode potential given by metallic Li ($Li^0$).

For $Li_xRuO_3$, the calculated intercalation potential is positive for all values $0<x\leqslant 2$, giving, technically, a capacity of

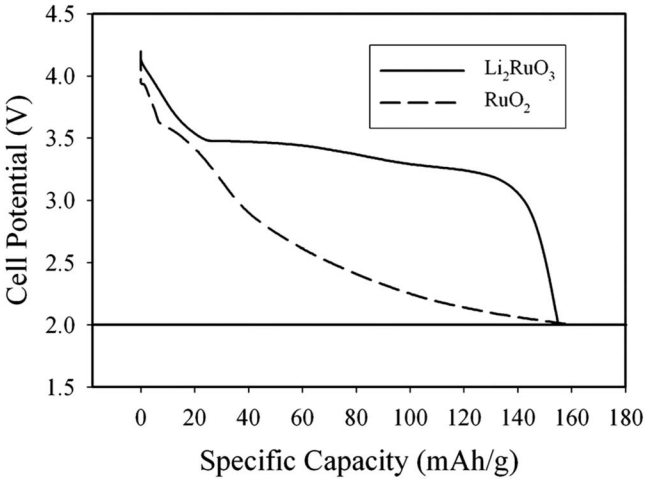


FIG. 3. Experimental discharge curves for $Li_xRuO_3$ and rutile $Li_xRuO_2$. The two lines are labeled according to the synthesized compound, which corresponds to the discharged end point for the layered material and the charged end point for the rutile material.

two Li ions per Ru ion. However, it is unlikely that the Li ions in the metal-oxide plane can be deintercalated without destabilizing the structure. Therefore, 1.5 Li per Ru ion is a more reasonable estimate of the capacity. Deintercalation has been demonstrated to almost exactly this limit.[3] The capacity limit for rutile $Li_xRuO_2$ is determined not by how much Li can be deintercalated, but rather by how much Li the compound can hold. A clear experimental evaluation of this limit is complicated by the existence of the alternate chemical reaction by which Li combined with $RuO_2$ decomposes to form metallic Ru and $Li_2O$ instead of intercalating into the rutile structure. One early report indicates that 1.3 Li ions can be intercalated into the rutile $RuO_2$ lattice.[4] A more recent report demonstrated that both reactions (intercalation and decomposition) occur, but that decomposition dominates above 1.2 V.[5] Our calculated intercalation potential remains positive until the lattice contains approximately 1.2 Li, in very good agreement with available experimental evidence.

Our measured values for potential for $Li_xRuO_3$ and $Li_xRuO_2$ during discharge as a function of specific capacity are shown in Fig. 3. Note that the compounds, as synthesized, are in different states: $Li_2RuO_3$ is a discharged cathode that must be deintercalated before use, while $RuO_2$ is a fully charged cathode. To compare these to our calculated values, we note that surfaces and grain boundaries, which are not modeled in our calculations, can have a strong effect on the measured potential. Therefore, we ignore the first 10–15 mA h/g of data where these effects are most likely to dominate.

The average potential for layered $Li_xRuO_3$ throughout the discharge curve (above 15 mA h/g) is about 3.4 V, in very good agreement with our calculated average value for the entire Li range $V(\bar{x}=1.0)=3.5$ V (note the different scale on the voltage axes of the theoretical and experimental plots).

For $Li_xRuO_2$, the experimental average voltage is about 2.5 V. A direct comparison with our calculated value is difficult because only the topotactic intercalation is considered, whereas the intercalational and decompositional reactions cannot be definitively separated in our experimental data. Reference 5 reports that intercalation takes place in a limited voltage range between 0.5 and 1.2 V, although Ref. 4 finds voltages up to 2.3 V in samples that still exhibit the rutile structure. It is likely, then, that most or all of the voltages for the $Li_xRuO_2$ discharge shown in Fig. 3 come from the nontopotactic (decompositional) alternate chemical reaction and cannot be directly compared to Fig. 2.

The most important results to emerge from our calculations are that Li intercalates into the rutile structure at a much lower voltage than into the layered structure, the decrease of voltage during discharge is sharper for the rutile compound, and that the capacities of the two cathodes are similar (1.2 Li vs 1.5 Li). Both these facts and the values of the average intercalation potentials are in very good agreement with our measurements and with previously reported measurements.[3–5]

## V. FIRST PRINCIPLES ANALYSIS

The good agreement between theory and experiment allows us to investigate, from a first principles perspective, the intriguing question of why two compounds that contain the same constituent atoms have such different voltage behaviors. The threefold answer to this question will be addressed part by part in the following sections.

### A. Oxidation state

The higher oxidation state of $Li_xRuO_3$ compared to $Li_xRuO_2$ at the same $x$ is the first significant contribution to the higher voltage. Since one out of every three Ru atoms in the metal-oxide plane is replaced by a Li atom in $Li_2RuO_3$, each Ru ion must donate more electrons per O atom than its counterpart in rutile $Li_xRuO_2$. The Li atoms located in the Ru plane are unlikely to be exchanged during cycling because it would too strongly destabilize the structure. (This contention is supported by experimental data, which show that only 1.5 Li ions can be extracted from the structure,[3] exactly the number required to leave only the metal-oxide plane Li's). Based on this, we understand the "empty" lattice for the layered compound to be $Li_{0.5}RuO_3$, which gives a formal valency of $Ru^{5.5+}$ $(=d^{2.5})$ compared to $Ru^{4+}$ $(=d^4)$ for the empty rutile structure $RuO_2$. As the Ru oxidation state is increased, the negatively charged $O^{2-}$ ion experiences a more positive Coulomb field from the Ru ion and the $2p$ states shift down in energy; a similar effect is operative for the $d$ states of Ru, which are less shielded from the positive Ru ion core and also shift down. As electrons enter the host lattice during discharge, the $p$ and $d$ states move upward in energy concurrent with the decreasing oxidation state of the electrochemically active ion. This shrinks the energy separation between the highest occupied Li states in the anode and the lowest unoccupied $d$ states of the cathode, thereby lowering the potential. A schematic of the relevant orbitals in the anode and cathode in Fig. 4 shows the energy difference, $\Delta E$, between an electron's original and final states during discharge for two different oxidation states. $\Delta E$ is directly related to the intercalation potential, which is, therefore, directly related to

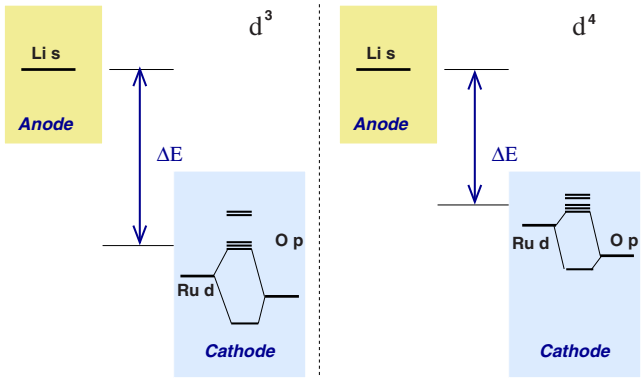


FIG. 4. (Color online) A schematic showing the energy difference between the highest occupied electronic state in the anode and the lowest unoccupied state in the cathode for different oxidation states of the Ru ion. The bonding and/or antibonding between O $p$ and Ru $d$ states is also shown, along with the $t_{2g}-\epsilon_g$ split (the $t_{2g}$ are the lower, threefold degenerate complex; the $\epsilon_g$ are the upper twofold degenerate complex) that results from the octahedral environment of the Ru ion. For both $Li_xRuO_3$ and $Li_xRuO_2$ at all $x$, the electrons enter the $t_{2g}$ complex. The $d^4$ state corresponds to fully charged rutile $Li_xRuO_2$ ($x=0$) and fully discharged layered $Li_xRuO_3$ ($x=2$). The discharged rutile compound has a $d^5$ configuration, while the charged layered compound has a $d^{2.5}$ configuration. Further splittings of the $t_{2g}$ complex are discussed in Sec. V C.

the oxidation state of Ru. At a given $x$, the Ru ion of the rutile structure contains 1.5 more electrons than that of the layered structure. The resultingly higher $d$ bands strongly decrease the intercalation potential in comparison. It is interesting to note that the fully discharged layered compound ($Li_2RuO_3$) has a Ru ion with the same oxidation state as the fully charged rutile compound ($RuO_2$) and that the top of the theoretical rutile discharge curve has a very similar voltage to the bottom of the layered curve.

Also shown in Fig. 4 is the effect that the Ru-O bonding has on the energy levels. The overlap between Ru $d$ states and O $p$ states causes an upward shift of the former and a downward shift of the latter (antibonding, bonding). A stronger overlap of the two orbitals will increase the antibonding, shift up the $d$-derived levels, and lower the intercalation potential. In the two empty lattices, the Ru-O distances (which measure the orbital overlap) are fairly similar: 1.95 Å for $Li_{0.5}RuO_3$ and 1.97 Å for $RuO_2$. As Li is intercalated into the hosts, the overlap decreases because the O atoms move away from the growing negative charge around the Ru ion. At a given $x$, the Ru-O overlap will be larger in the layered compound due to its higher oxidation state (less negative Ru ion). This effect acts in opposition to the shift of the $d$ band complex as a function of oxidation state, but is evidently weaker as the overall effect of reducing the Ru ion is to lower the intercalation potential.

As a general principle, a high oxidation state of the electrochemically active ion in a cathode will raise the voltage compared to a lower oxidation state. Further investigation of structures with a low $M/O$ ratio ($M$=electrochemically active metal ion) may prove fruitful in developing high energy cathode materials.

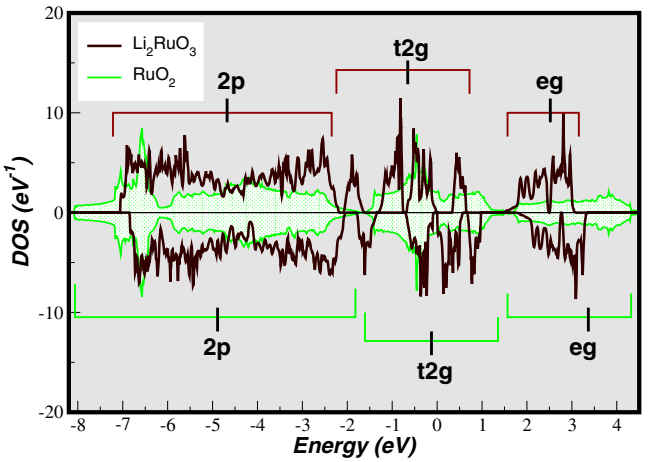


FIG. 5. (Color online) The DOS of $Li_2RuO_3$ and $RuO_2$; the spin majority spectrum is on the positive $y$ axis and the spin minority spectrum is on the $-y$ axis. The sharper, more localized states of $Li_2RuO_3$ are due to the two-dimensionality of bonding in the layered structure, while the broad, metallic states of $RuO_2$ are due to nearly isotropic bonding in the rutile lattice. The splitting of the $t_{2g}$ complex is due to Ru-Ru bonding (see text).

### B. Dimensionality

The voltage offset between $RuO_2$ and $Li_2RuO_3$ during discharge can be attributed partially to different oxidation states, as discussed above, but also to differences in bonding that stem from their respective dimensionalities. In both structures, the electrochemically active Ru ion is in an octahedral (or distorted octahedral) environment of surrounding O ions, and in both cases, the Ru-O distances are very similar, but the octahedra in layered $Li_2RuO_3$ are edge sharing in the two-dimensional metal-oxide plane and unattached to octahedra in the adjacent plane, while in the rutile lattice, the octahedra are edge sharing in two directions and attached by corners in the third direction (see Fig. 1). In the edge-sharing configuration, the Ru-O-Ru bonds are nearly 90°, while in the corner-sharing configuration, the angle is nearly 180°. Two Ru ions connected through edge-sharing octahedra cannot $\sigma$-bond with a single $p$ orbital on the shared O site. However, at a shared corner, the same O $p$ orbital has a $\sigma$-like overlap with both neighboring Ru ions. Thus, $RuO_2$ not only has an extra dimension of bonding, but the manner in which the octahedra are connected is much more favorable for hopping. The strongly increased bonding afforded by the rutile structure widens the energy levels into broader bands than in the layered structure. As can be seen in Fig. 5, the $RuO_2$ density of states (DOS) is broad and low, whereas the $Li_2RuO_3$ DOS is comparatively sharp and narrow. The octahedral environment of the Ru ion in both compounds splits the $d$ states into a lower threefold degenerate set, $t_{2g}$, and a higher twofold degenerate set, $\epsilon_g$. Ru-Ru bonding (discussed in the next section) further splits the $t_{2g}$ states in $Li_2RuO_3$ and exaggerates the bandwidth of this complex. The $\epsilon_g$ states are much less affected and provide a good quantitative comparison to $LiRuO_2$. Figure 5 shows that the $\epsilon_g$ states in $LiRuO_3$ are 1.55 eV wide, whereas in $LiRuO_2$, they are 3.27 eV wide, more than a factor of 2 greater. From the

perspective of electrochemical performance, a more metallic (broader bandwidth) system has both advantages and disadvantages. There are no energy gaps between redox couples in a metal and, therefore, electrical conduction, often a barrier to good battery cycling, is better throughout the full range of Li contents. However, the trade-off is that the intercalation potential is lowered because the top of a broadened band complex will exist at a higher energy than the top of a more localized one, decreasing $\Delta E$ and reducing the potential. Consequently, the bottom of the complex will be lower, but electrons are removed from the highest energy states first and rarely can enough Li be removed from any compound to exploit the lowest states.

In intercalated rutile $RuO_2$ the voltage is lower overall than in layered $Li_2RuO_2$, but also decreases much more quickly as a function of Li content. The sharp drop-off in voltage seen in Fig. 2 can also be explained in terms of dimensionality. When $Li_2RuO_3$ is deintercalated such that only one Li ion per Ru ion is in the lattice ($LiRuO_3$), the broad Li plane can be arranged such that the two nearest Li ions are 5.27 Å apart. In the rutile structure, intercalation of one Li ion ($LiRuO_2$) into the "pocket" between $RuO_6$ octahedra requires that Li ions sit merely 2.77 Å from one another. The Coulomb penalty for two positive $Li^+$ ions so close together raises the total energy of the compound and decreases the intercalation potential [see Eq. (1)]. Remarkably, even when two Li ions per Ru occupy the layered structure, the nearest neighbor Li's still sit slightly farther apart (2.80 Å) than nearest neighbor Li's in the rutile structure with only one Li per Ru.

### C. Ru-Ru bonding

Finally, we discuss the effects of strong Ru-Ru bonding that occurs in $Li_xRuO_3$. No such bonding is observed in rutile $RuO_2$, although other rutile compounds such as $NbO_2$ or $MbO_2$ do exhibit metal-metal bonding.[14] In $Li_xRuO_3$, the Ru ions in the metal-oxide plane are observed to dimerize into pairs, lowering the in-plane symmetry from the original triangular configuration[3,12,13] [see Fig. 6(a)]. In our calculations, this dimerization persists as the compound is delithiated until the phase transition to rhombohedral symmetry occurs. A recent paper[19] finds a different Ru-Ru bonding configuration than the one reported in Refs. [3,12,13] and the one examined here, but the result is still one long and two short bonds for each Ru ion, and an increased overlap between orbitals with short bonds as described below. We have not investigated this alternate dimerization pattern, but the energy level structure we discuss here would be precisely the same.

As the two Ru ions draw together, adjacent $d_{xy}$ [in the local coordinates of Fig. 6(b)] orbitals experience an increased $\sigma$ overlap and strongly bond or antibond to form two molecular orbitals. The other $t_{2g}$ states, $d_{xz}$ and $d_{yz}$, also form bonding or antibonding states (of $\pi$ and $\delta$ types, respectively) with adjacent orbitals, although the split is considerably weaker than for $d_{xy}$. A schematic of the energy splittings due to Ru-Ru bonding is shown in Fig. 6. Note that the $d_{xz}$ and $d_{yz}$ bonding or antibonding states are, in reality, slightly

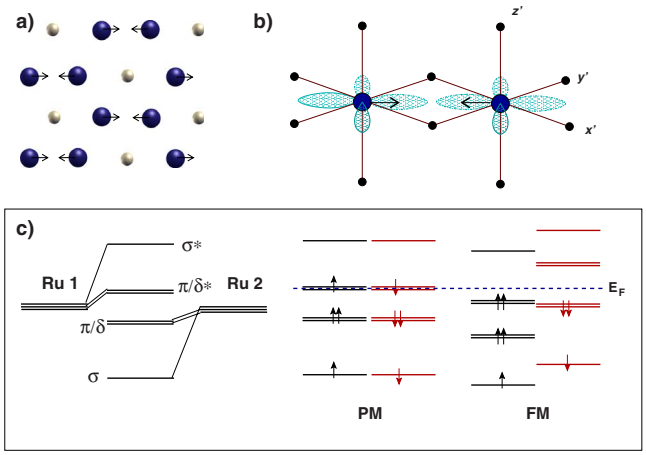


FIG. 6. (Color online) (a) The Ru/Li plane of $Li_2RuO_3$ in the (100) metal plane. The dimerized pairs of Ru atoms draw in toward one another as indicated by arrows. (b) Two adjacent edge-sharing $RuO_6$ octahedra showing the $d_{xy}$ orbitals that form strong bonding or antibonding states upon dimerization. (c) The spectrum of energy levels resulting from bonding and antibonding between the two dimerized Ru ions is shown, along with the paramagnetic (PM) and ferromagnetic (FM) configurations for $x=2$. The spin-polarized state allows for a gap to form at the Fermi energy and lowers the overall energy. The configuration for $LiRuO_3$ can be visualized by removing the two top electrons from the PM configuration of $Li_2RuO_3$.

split from each other (due to the difference between $\pi$ and $\delta$ bondings), but are drawn as degenerate because the broadening of the states into bands in the solid obscures the gap and renders the two states quasidegenerate (see Fig. 7). The energy configuration resulting from Ru-Ru bonding has ramifications both for the conductivity and for the ground state magnetism.

In $Li_2RuO_3$, the splitting of the $t_{2g}$ complex, followed by a subsequent exchange splitting, allows for a small gap to form at $E_F$. As shown in Fig. 6, the eight electrons of the two dimerized $Ru^{4+}$ ($=d^4$) ions fill the paramagnetic states such that the Fermi energy cuts through the doubly degenerate antibonding pair, $\pi/\delta^*$. This causes the Fermi energy to cut through the middle of the band complex. If the states of one spin type are shifted down, two majority spin electrons can sit beneath $E_F$, while the two emptied minority states sit above $E_F$, leaving a gap equal to the exchange energy between filled and empty states. Spin unrestricted calculations yield the expected magnetic ground state with an exchange splitting of approximately 1 eV (though various magnetic ordering patterns may be possible, only the ferromagnetic possibility was investigated here). Broadening of the electron states into bands in the solid reduces the gap such that $Li_2RuO_3$ is a very narrow gap semiconductor (~7 meV) with the gap between opposite spin states (see Fig. 7). The energetic advantage of spin polarization should disappear once the compound is delithiated to $LiRuO_3$ because the six electrons of the two $Ru^{5+}$ ions ($d^3$) fill both quasidegenerate bonding levels ($\pi/\delta$), leaving a gap between the $\pi/\delta$ and $\pi/\delta^*$ states. Spin unrestricted calculations for this system, indeed, find a paramagnetic ground state. Since the $\pi/\delta$

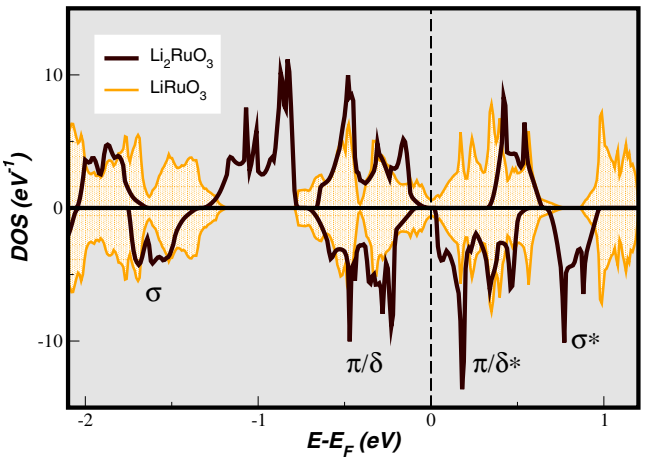


FIG. 7. (Color online) DOS plot for the $t_{2g}$-originated complex of $Li_2RuO_3$ and $LiRuO_3$ with their respective Fermi energies shifted to 0 eV; spin majority states are shown on the positive $y$ axis and spin minority states are shown on the negative $y$ axis. Only the $t_{2g}$-derived states are within the energy boundaries of the plot; $\varepsilon_g$-derived states and the $O_p$ states are higher and lower in energy, respectively. The energy splittings due to Ru-Ru bonding are easily identifiable for $Li_2RuO_3$. For $LiRuO_3$, the symmetry is lowered by the removal of one Li and the states that were twofold degenerate in the fully lithiated compound are split. All states have been shifted such that the Fermi energy coincides with 0 eV.

bonding or antibonding is rather weak (certainly weaker than the exchange splitting), the predicted gap is overcome by the broadening of the states in the crystal and the system becomes semimetallic. The results of our calculations are consistent with experimental measurements that show semiconducting behavior for $Li_2RuO_3$ and very weakly semiconducting or nearly metallic behavior for $LiRuO_3$.[13] Without Ru-Ru bonding and the concurrent energy level splitting, the degenerate electron states of the $t_{2g}$ complex would be partially filled for all $x$ in the $Li_xRuO_3$ series, as is the case for the rutile $Li_xRuO_2$. Measurements of the conductivity of $RuO_2$ show that it is 2 orders of magnitude more conductive at low temperature than $Li_2RuO_3$.[13,20] The magnetic ground state of $Li_2RuO_3$ and the paramagnetic ground state of $LiRuO_3$ also match well with experimental measurements of susceptibility. In $Li_2RuO_3$, a Curie-Weiss-like curve is seen,[12] whereas in $LiRuO_3$, a Pauli-like behavior is observed.[13] If the $t_{2g}$ complex were intact (i.e., no Ru-Ru bonding), one would expect that if a local magnetic moment formed for $Li_2RuO_3$ ($d^4$, $\mu=2$), then it would also form for $LiRuO_3$ ($d^3$, $\mu=3$).

The stability of the $Li_xRuO_3$ compound series may also be affected by Ru-Ru bonding. The compound $LiNiO_2$ is structurally very similar to $LiRuO_2$: stacked metal-oxide planes in a rhombohedral symmetry with Li planes in between. In the nickelate compound, Ni ions migrate into the Li plane during deintercalation due to the similar ionic radii of $Ni^{3+}$ and $Li^+$ ions. This migration has deleterious effects on cycling properties because it strongly inhibits Li-ion mobility.[21] The ionic radius of $Ru^{4+}$ is even closer to that of $Li^+$ than $Ni^{3+}$, but no off-stoichiometry version of $Li_xRuO_3$ has been reported and the system has very good cycling properties.[22] This may be due to the Ru-Ru bonding, which makes it energetically unfavorable for one of a dimerized pair of Ru ions to break its bond and migrate into the Li plane.

## SUMMARY

We have synthesized layered $Li_2RuO_3$ and rutile $RuO_2$ and shown, using first principles theory, that their voltage profile and capacities are well reproduced within the ranges where comparison is possible. By analyzing the basic chemical and physical principles that contribute to differences between the properties of the two compounds, we can extract several underlying factors that determine the very different properties of the two materials. First, we find that a high oxidation state of the electrochemically active metal ion gives rise to a high voltage by shifting the metal $d$ states downward in energy. Second, low dimensionality allows for increased localization of the electron states (compared to three-dimensional systems), which, in turn, gives rise to higher voltage. A two-dimensional intercalation plane also provides a larger area for Li ions to disperse into, thereby lowering the energy penalty of Li-Li interactions. Finally, we find that Ru-Ru bonding in $Li_2RuO_3$ plays a crucial role in determining the conductivity by lowering the symmetry and allowing a narrow gap to form at the Fermi energy. Without this kind of bonding in $RuO_2$, the $t_{2g}$ states remain degenerate and good metallic conduction is observed. Though Ru-Ru bonding is specifically relevant only to $Li_2RuO_3$, a search for superior cathode materials can easily incorporate a high oxidation state, possibly derived from a low metal/oxygen ratio and strong two-dimensionality as general principles.

## ACKNOWLEDGMENTS

We acknowledge our several very enlightening discussions with J. Goodenough as well as helpful conversations with I. I. Mazin. Research at NRL is supported by the Office of Naval Research. M.D.J. would like to acknowledge use of computing resources at the ASC HPC.

[1] M. K. Aydinol, A. F. Kohan, G. Ceder, K. Cho, and J. Joannopoulos, Phys. Rev. B **56**, 1354 (1997).

[2] In Ref. 1, the overall Bravais lattice and symmetry were held constant, but the atoms were allowed to relax to their lowest energy position. This relaxation was shown to be important for good agreement between experimental and theoretical intercalation potentials.

[3] H. Kobayashi, R. Kanno, Y. Kawamoto, M. Tabuchi, O. Nakamura, and M. Takano, Solid State Ionics **82**, 25 (1995).

[4] D. W. Murphy, F. J. Di Salvo, J. N. Carides, and J. V. Waszczak,

Mater. Res. Bull. **13**, 1395 (1978).
[5] P. Balaya, H. Li, K. Lorentz, and J. Maier, Adv. Funct. Mater. **13**, 621 (2003).
[6] P. E. Blochl, Phys. Rev. B **50**, 17953 (1994).
[7] G. Kresse and D. Joubert, Phys. Rev. B **59**, 1758 (1999).
[8] G. Kresse and J. Furthmuller, Phys. Rev. B **54**, 11169 (1996).
[9] J. P. Perdew, J. A. Chevary, S. H. Vosko, K. A. Jackson, M. R. Pederson, D. J. Singh, and C. Fiolhais, Phys. Rev. B **46**, 6671 (1992).
[10] G. Ceder, M. K. Aydinol, and A. F. Kohan, Comput. Mater. Sci. **8**, 161 (1997).
[11] F. Zhou, M. Cococcioni, C. A. Marianetti, D. Morgan, and G. Ceder, Phys. Rev. B **70**, 235121 (2004).
[12] A. C. W. P. James and J. B. Goodenough, J. Solid State Chem. **74**, 287 (1988).
[13] H. Kobayashi, R. Kanno, Y. Kawamoto, M. Tabuchi, and O. Nakamura, Solid State Ionics **86**, 859 (1996).
[14] N. Beatham and A. F. Orchard, J. Electron Spectrosc. Relat. Phenom. **16**, 77 (1979).
[15] G. J. Moore, C. S. Johanson, and M. M. Thackeray, J. Power Sources **119-121**, 216 (2003).
[16] R. Wartena, A. E. Curtright, C. B. Arnold, A. Pique, and K. E. Swider-Lyons, J. Power Sources **126**, 193 (2004).
[17] C. Wolverton and A. Zunger, Phys. Rev. Lett. **81**, 606 (1998).
[18] P. D. Tepesch, G. D. Garbulsky, and G. Ceder, Phys. Rev. Lett. **74**, 2272 (1995).
[19] Y. Miura, Y. Yasui, M. Sato, N. Igawa, and K. Kakurai, J. Phys. Soc. Jpn. **76**, 033705 (2007).
[20] W. D. Ryden, A. W. Lawson, and C. C. Sartain, Phys. Rev. B **1**, 1494 (1970).
[21] K. Kang, Y. S. Meng, J. Berger, C. P. Grey, and G. Ceder, Science **311**, 977 (2006).
[22] A. M. Stux and K. E. Swider-Lyons, J. Electrochem. Soc. **152**, A2009 (2005).